Toxicology in Vitro 65 (2020) 104815

Contents lists available at ScienceDirect

Toxicology in Vitro

journal homepage: www.elsevier.com/locate/toxinvit

Microfluidic chip for culturing intestinal epithelial cell layers: Characterization and comparison of drug transport between dynamic and static models

Kornphimol Kulthong[a,b,c], Loes Duivenvoorde[b], Huiyi Sun[b], Samuel Confederat[b], Jiaqing Wu[a], Bert Spenkelink[a], Laura de Haan[a], Victor Marin[b], Meike van der Zande[b,1], Hans Bouwmeester[a,*,1]

[a] Division of Toxicology, Wageningen University, P.O. box 8000, 6700 EA Wageningen, the Netherlands
[b] Wageningen Food Safety Research, P.O. Box 230, 6700 AE Wageningen, the Netherlands
[c] National Nanotechnology Center (NANOTEC), National Science and Technology Development Agency, Pathum Thani 12120, Thailand

ARTICLE INFO

Keywords:
Microfluidics
Gut-on-chip
Dynamic flow
Transport
Bioavailability

ABSTRACT

Dynamic flow *in vitro* models are currently widely explored for their applicability in drug development research. The application of gut-on-chip models in toxicology is lagging behind. Here we report the application of a gut-on-chip model for biokinetic studies and compare the observed biokinetics of reference compounds with those obtained using a conventional static *in vitro* model. Intestinal epithelial Caco-2 cells were cultured on a porous membrane assembled between two glass flow chambers for the dynamic model, or on a porous membrane in a Transwell model. Confocal microscopy, lucifer yellow translocation, and alkaline phosphatase activity evaluation revealed that cells cultured in the gut-on-chip model formed tight, differentiated, polarized monolayers like in the static cultures. In the dynamic gut-on-chip model the transport of the high permeability compounds antipyrine, ketoprofen and digoxin was lower (*i.e.* 4.2-, 2.7- and 1.9-fold respectively) compared to the transport in the static Transwell model. The transport of the low permeability compound, amoxicillin, was similar in both the dynamic and static *in vitro* model. The obtained transport values of the compounds are in line with the compound Biopharmaceuticals Classification System. It is concluded that the gut-on-chip provides an adequate model for transport studies of chemicals.

1. Introduction

Toxicological safety studies of pharmaceuticals and industrial chemicals are an integral part of product development. Traditionally, this implies the use of animals, which not only is time consuming, considered unethical and expensive, but importantly also raises scientific questions related to interspecies differences in biokinetics compared to humans (Martignoni et al., 2006; Leppert et al., 2006). The combination of these scientific, socioeconomic, and ethical concerns resulted in attempts to refine, reduce, or replace (3Rs) the use of animals for toxicological safety studies (Matthiessen et al., 2003; Russell and Burch, 1959; Rollin, 2003; Eisenbrand et al., 2002). Since the launch of the 3Rs principle several *in vitro* models have been proposed as alternative models to reduce animal experiments to study drug permeation across the intestinal epithelium (Kauffman et al., 2013; Guerra et al., 2010; Cao et al., 2015).

More recently and along these lines, dynamic flow gut-on-chip devices have been proposed as an additional tool to existing static *in vitro* cell culture models. The devices mimic *in vivo* tissue to fluid ratios and fluid flow by using microfluidic technology (Kim et al., 2012; Kim and Ingber, 2013) attempting to better recapitulate the *in vivo* physiological tissue functioning. An additional advantage of gut-on-chip devices for compound transport and effect studies is that they allow for integrated online detection (Gao et al., 2013; Santbergen et al., 2019) and coupling to other organ-on-chip systems (Mahler et al., 2009; Lee et al., 2017a). Gut-on-chip models have been proposed for preclinical (Chi et al., 2015; Kim and Ingber, 2013; Kim et al., 2012; Shim et al., 2017) and pharmacological applications (Gupta et al., 2016; Barata et al., 2016; Selimovic et al., 2011). To emulate human intestinal disease models human stem cell-based intestinal models have been used (Workman et al., 2018). However, given the yet unresolved issues on reproducibility and lab variability in stem cell models, cell line based

* Corresponding author.
E-mail address: hans.bouwmeester@wur.nl (H. Bouwmeester).
[1] These authors jointly directed this work.

https://doi.org/10.1016/j.tiv.2020.104815
Received 21 January 2020; Accepted 28 February 2020
Available online 29 February 2020

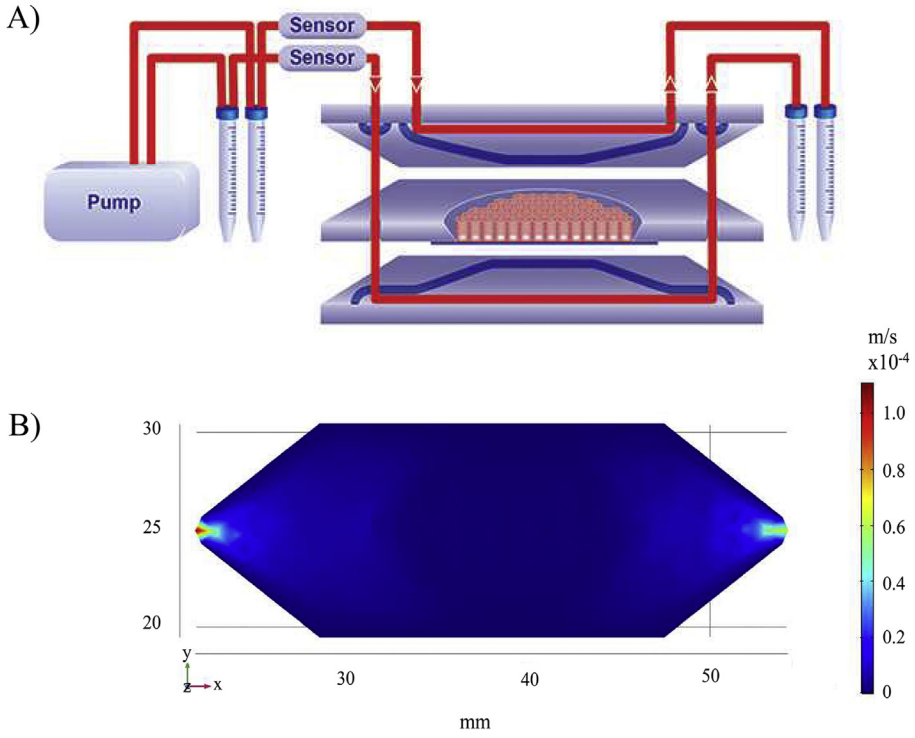

Fig. 1. *Experimental setup of the gut-on-chip* A) Schematic design of the microfluidic system. B) Flow velocity simulation of the apical chamber using COMSOL. A horizontal cross-section was taken indicating a steady value of flow velocity inside the flowcell, within the laminar regimen. The picture shows a lower flow speed at the centre of the device.

models are preferred for toxicokinetic and toxicodynamic studies (Ortmann and Vallier, 2017).

The transport of several compounds has been evaluated using variants of gut-on-chip models, notably: antipyrine, propranolol, naproxen, furosemide, verapamil, atenolol, piroxicam, hydrochlorothiazide, cimetidine, carbamazepine (Yeon and Park, 2009), acetaminophen (Mahler et al., 2009; Marin et al., 2019; Lee et al., 2017a), rhodamine 123 (Kimura et al., 2008) and curcumin (Gao et al., 2013). Only for a limited number of compounds the transport in a dynamic gut-on-chip model has been compared to that in the conventional Transwell model. These studies have been performed for caffeine, atenolol (Pocock et al., 2017), cyclophosphamide (Imura et al., 2009), mannitol, insulin (Tan et al., 2018) acetaminophen (Marin et al., 2019), verapamil, ergotamin (in)e, food contaminant compounds (Santbergen et al., 2020), and the environmental contaminants of the dioxin and PCB group (Kulthong et al., 2018). The observed transport of the compounds in the dynamic gut-on-chip models were consistent with those obtained using a conventional Transwell for most compounds, with the exception of caffeine (higher transport in gut-on chip), atenolol (higher transport) and ergotaminine (lower transport).

Most gut-on-chip devices are manufactured using polydimethylsiloxane (PDMS). This is mainly because PDMS is biologically compatible and allows soft lithography-based production methods, which enable rapid manufacturing of three-dimensional microstructures, (McDonald et al., 2000; Thangawng et al., 2007; Tsao, 2016). In addition PDMS-based devices allow microscopy-based readouts (Berthier et al., 2012). However, PDMS has a major disadvantage; it adsorbs a wide range of molecules such as proteins and lipophilic drugs (Hirama et al., 2019; Berthier et al., 2012; Li et al., 2009). Adsorption can partially be prevented by applying a coating on the PDMS (van Meer et al., 2017), but this might influence the outcome of a biological study. Therefore, in our studies we used a microfluidic gut-on-chip device that consists of three resealable glass slides that, upon assembly, result in two flow chambers separated by a middle layer that contains a porous cell culture membrane.

In this study, we aimed to evaluate whether our *in vitro* gut-on-chip intestinal barrier model is an adequate model for compound transport studies. To this end we performed a biokinetic study comparing a dynamic gut-on-chip (Kulthong et al., 2018) with a conventionally used static Transwell model. We exposed Caco-2 cells, grown in the gut-on-chip or Transwell model to several model compounds for which extensive information on *in vivo* bioavailability and transport mechanisms is available. High and low oral permeability class compounds were selected, known to represent different absorption mechanisms (*e.g.* passive diffusion and active transport). For these drugs we determined permeability coefficients using both models. In addition, a morphological and functional characterization of the dynamic gut-on-chip and static Transwell models was performed using confocal microscopy and enzyme activity assays. We report the influence of laminar flow on compound transport, which was evaluated in the gut-on-chip under static and dynamic conditions.

2. Materials and methods

2.1. Chemicals and reagents

Antipyrine, ketoprofen, digoxin, amoxicillin, bovine serum albumin (BSA), Dulbecco's Modified Eagle Medium (DMEM), penicillin-streptomycin, Hank's balanced salt solution (HBSS), trifluoroacetic acid were obtained from Sigma-Aldrich (Zwijndrecht, The Netherlands). Phosphate Buffered Saline (PBS), heat inactivated fetal bovine serum (FBS) and MEM-non-essential amino acids were purchased from Fisher Scientific (Landsmeer, The Netherlands). Amoxicillin-d4 was obtained from CacheSyn (Mississauga, Canada). Acetonitrile was obtained from Biosolve (Valkenswaard, The Netherlands). Formic acid was purchased form VWR international (Darmstadt, Germany).

2.2. Design of the gut-on-chip system

The microfluidic gut-on-chip device has been described before (Kulthong et al., 2018). In short, it consists of three 15 × 45 mm (width × length) re-sealable glass slides that result in two flow chambers (*i.e.* an upper apical (AP) and lower basolateral (BL) chamber) upon assembly (see Fig. 1A; Micronit, Enschede, The Netherlands). Both the

upper and lower glass slides were spaced from the middle layer membrane by a 0.25 mm thick silicone gasket and the flow chambers were separated by a glass slide containing a porous cell culture membrane that was fixed on the glass slide. The membrane consisted of a polyester (PET) membrane with a 0.4 μm pore size and a 1 cm^2 surface area. The height of the cell culture area was 0.65 mm and the height of the bottom flow channel was 0.25 mm, resulting in a volume of 110 mm^3 and 75 mm^3 for the AP and BL side, respectively, and 185 mm^3 for the total volume of the device (μL). The chip was placed in a chip holder with a quick locking mechanism, constructed for connection of external capillaries to the chip *via* specific ferrules to ensure tight connections and a leak-free system.

The flow was induced using a multi-channel air pressure driven pump. Two channels per chip (*i.e.* one for the AP side and one for the BL side) were connected to the chip inlets using Polyetheretherketone (PEEK) capillary tubing (0.125 mm inner diameter, with a total length of 60 cm). Each flow channel was equipped with a flow sensor to assure precise regulation of the flow, which was located at 40 cm distance from the pump and 20 cm distance from the chip. Fluorinated Ethylene Propylene (FEP) tubing (0.250 nm inner diameter, 40 cm length) was used to connect to the chip outlets to the culture medium reservoirs. Before the start of each experiment, all tubing and chips were sterilized using an autoclave and rinsed with 70% ethanol. Tubing and chips were prefilled with medium to eliminate air bubbles in the system. The entire system was put in an incubator at 37 °C to maintain cell culture conditions.

2.3. Cell culture

A Caco-2 cell line (HTB-37), derived from a human colorectal adenocarcinoma, was obtained from the American Type Culture Collection (ATCC, Manassas, VA, USA). The cells were grown (at passage number 29–45) in complete culture medium, consisting of DMEM supplemented with 10% FBS, 1% penicillin-streptomycin, and 1% MEM non-essential amino acid, further referred to as $DMEM^+$.

The cells were seeded at a density of 75,000 cells per cm^2 on 12-well Transwell polyester inserts (0.4 μm pore size, 1.12 cm^2 surface area, Corning Amsterdam, The Netherlands) and cultured in $DMEM^+$ for 21 days. The medium was changed every two to three days.

In the microfluidic chip, the cells were seeded at a density of 75,000 cell per cm^2 and were allowed to attach to the membrane. After 24 h the membrane was inserted in the microfluidic chip. After attachment, the cells were exposed to a continuous flow of 100 μL/h $DMEM^+$ for 21 days. By doing so, the shear stress in the AP compartment was ~0.0002 dyn/cm^2 at the membrane surface, where the cells are grown. The $DMEM^+$ medium contained sodium bicarbonate (10 mM) to optimize the pH buffering capacity.

2.4. Caco-2 monolayer integrity

Apical to basal translocation of lucifer yellow was measured in a Caco-2 monolayer under static and dynamic conditions. A lucifer yellow solution of 500 μg/mL in $DMEM^+$ was perfused through the apical channel of the chip with a flow rate of 100 μL/h. The basolateral channel was perfused with $DMEM^+$ with a flow rate of 100 μL/h. Sample aliquots of 50 μL were collected from the apical and basal outlet every half hour for 3 h. The same concentration of lucifer yellow solution was added apically to the cells in a Transwell (500 μL/insert) and incubated for 1 h before collecting the medium sample from the apical and basolateral chambers. The fluorescence intensity (485/530 nm) of all collected samples from both systems was measured using a microplate reader (Synergy HT, BioTek, VT).

2.5. Fluorescent imaging of in vitro epithelial cell morphology

Twenty-one days after seeding, Caco-2 cells, grown in the gut-on-chip or Transwell, were prepared for cell and monolayer morphological assessment. The chips were opened, and cells were fixed with 4% formaldehyde at room temperature for 10 min and rinsed with PBS. Cells were then permeabilized with 0.25% Triton X100 in PBS for 10 min, rinsed with PBS and blocked with 1% acetylated bovine serum albumin in PBS for 30 min. Tight junctions were stained with 10 μg/mL conjugated antibody ZO-1/TJP1-Alexa Fluor 594 (Invitrogen, Waltham, MA). The nuclei were stained with 5 μg/mL DAPI (Invitrogen, Waltham, MA) and 4 U/mL Phalloidin Alexa Fluor 488 (Life technologies, Carlsbad, CA) was used to stain actin filaments (*i.e.* cytoskeleton). The incubation time for all stainings was 30 min. Each membrane was then cut out and placed between two cover slips separated by a spacer (0.12 mm depth × 20 mm diameter) with a drop of anti-fading mounting medium on the membrane. The cells cultured on Transwell membranes were stained using the same procedure. The stained monolayers of cells were analysed using a confocal microscope (LSM 510 UVMETA; Carl Zeiss, Germany). Samples were excited with 405, 488 and 543 nm lasers. Multi-tracked images were captured to avoid bleed through. The used pinholes were in the range of 148–152 μm at a magnification of 40×. The gain and offset for the different channels were kept constant during the entire experiment.

2.6. Caco-2 differentiation

Alkaline phosphatase (ALP) activity was measured in cells cultured for 21 days in both systems using an ALP colorimetric assay kit (ab83369, Abcam, Cambridge, UK) following the protocol of the manufacturer. Briefly, the membranes/inserts were taken from the chip/Transwell chambers. After washing the cells with HBSS at 37 °C, trypsin/EDTA was added to the cells and they were incubated for 5–7 min. The cell suspension was collected and centrifuged at 300*g* for 5 min at 4 °C. The cell pellet was then resuspended in 200 μL ALP assay buffer and centrifuged at maximum speed, 16,000 RPM for 5 min at 4 °C. The supernatant (sample) was then collected and pipetted into the well of a 96-wells plate before adding the reaction buffer (50 μL/well), containing a *p*-nitrophenyl Phosphate solution (5 mM). After the plate was incubated in the dark for 60 min at 25 °C, 20 μL stop solution was added to each well of the reaction and shaken gently. Absorbance was read immediately at 405 nm using a microplate reader. A standard curve of p-nitrophenol (pNP) was prepared in a concentration range of 0–20 nmol/well, and converted to concentration after blank subtraction. Enzyme activity was calculated and expressed as nmol of pNP/min and normalised to the total amount of cells in term of protein content, which was measured using a RC-DC assay, a colorimetric protein determination based on the principle of Lowry estimation.

2.7. Computational model to calculate shear stress

Computational fluid dynamics was used to calculate the wall shear stress of the cell culture medium in the gut-on-chip using COMSOL Multiphysics® v. 5.3 (www.comsol.com, COMSOLAB, Stockholm, Sweden). The microfluidic device consisted of two rectangular microchambers separated by a glass middle layer containing a PET membrane. The inner dimensions of the rectangular chamber used for simulation consisted of one inlet and one outlet, the maximum inner high was 0.25 mm, the maximum width was 11 mm and length from inlet to outlet was 30 mm, and an oval cavity at the centre with area of 1.0 cm^2. Considering a steady flowrate of 100 μL/h we obtained laminar flow conditions with a Reynolds number of 0.007. The culture medium was considered as an incompressible and homogeneous, Newtonian fluid with similar conditions to water at 37 °C (density; 997 kg/m^3 and viscosity; 6.9×10^{-4} Pa s^{-1}). A laminar Flow/Stationary library was used to determine the shear rate. The shear stress was estimated by multiplying the shear rate with the dynamic viscosity of water at 37 °C. An extremely coarse mesh size was used to reduce the computing time. No-slip boundary conditions were applied to the microchannel walls.

Since the flow cell is fully made of glass, it was considered rigid with impermeable walls. The shear stress was obtained from the simulation using the height of 0.25 mm (near the inlet) and another position with an additional height of 0.40 mm at the centre of the chamber on the PET membrane. To corroborate this COMSOL calculation we used an adapted Poiseuille equation for rectangular microchannels as a second method (Zhang et al., 2014; Pocock et al., 2017). This equation could be applied to our system since the microfluidic chamber width is larger than the height (h < < w). To calculate the shear stress using this method two different heights were taken in consideration: 1) from the top to the glass middle layer (0.25 mm), and 2) from the top to the PET membrane (0.65 mm). Comparison of the COMSOL simulation and the adapted Poiseuille equation showed equal results.

2.8. Caco-2 viability

Cytotoxicity was assessed using an MTT assay, a mitochondrial activity-based cell viability assay. Caco-2 cells (50,000 cells/cm^2) were seeded in 96-well plates. After 24 h, the medium was discarded and was subsequently replaced with various concentrations of antipyrine (0, 25, 50, 100, 250 or 500 μM), ketoprofen (0, 25, 50, 100, 250 or 300 μM), digoxin (0, 25, 50, 100, 125 or 250 μM), or amoxicillin (0, 25, 50, 100, 250 or 500 μM) in HBSS for 24 h. At the end of the treatment period, cells were washed with 100 μL PBS, and 60 μL of 0.8 mg/mL MTT solution in DMEM$^+$ was added to the cells and further incubated for 1.5 h. The medium was then discarded, and the cells were permeabilized resulting in formazan crystals dissolving in 100 μL of DMSO. The absorbance was measured at 570 using a microplate reader and the background absorbance at 650 nm was subtracted. The percentage of cell viability was calculated from the absorbance obtained from the control divided by that of each treatment.

2.9. Compound transport studies across a monolayer of intestinal Caco-2 cells

The transport studies were performed following an established protocol for static transport studies using Caco-2 cells (Hubatsch et al., 2007). At day 21 post-seeding, a non-toxic concentration of 100 μM antipyrine, 100 μM ketoprofen, 125 μM digoxin, and 250 μM amoxicillin was prepared in a transport medium (HBSS).

In the gut-on-chip studies, each compound solution was perfused through the upper channel with a flow rate of 100 μL/h, whereas 4% BSA in HBSS was pumped through the basolateral channel. An aliquot (100 μL) was collected from the apical and basolateral outlet every hour for six hours.

In the Transwell studies, the cells were washed with HBSS for 15–20 min at 37° C (0.5 mL in apical side, and 1.5 mL in basolateral side). Subsequently, HBSS was removed from the basolateral chamber and replaced with 1.2 mL basolateral medium (4% BSA in HBSS). Compound solutions of 0.4 mL in HBSS were then added to the apical side of the inserts. From the basolateral side, aliquots (600 μL) were collected and replaced with the same volume of 4% BSA in HBSS at settled time points (0, 15, 30, 60, 90 and 120 min for antipyrine, ketoprofen and digoxin, and 0, 30, 60, 90, 120, 150 and 180 min for amoxicillin). All the liquid from the apical and basolateral chamber was collected at the last time point in order to calculate a mass balance. All samples were stored in −80 °C before analysis.

The transport was calculated from the experimental data using Eq. (1) for the Transwell data and (2) for the gut-on-chip data. Eq. (2) was derived from Eq. (1) (Yeon and Park, 2009).

$$P_{app} = \left(\frac{dQ}{dt}\right)\left(\frac{1}{AC_0}\right) \quad (1)$$

$$P_{app} = CV\left(\frac{1}{AC_0}\right) \quad (2)$$

Where A is the surface area (cm^2), dQ is the amount of the model compound transported (μmol) over the respective time interval, dt (s), C_0 is the initial concentration (μM), C is the concentration in the basolateral compartment (μM), and V is the flow rate (L/s).

2.10. Sample quantification (HPLC-UV/LC-MS/MS)

All samples from the transport experiments, except for the amoxicillin samples from experiments with cell monolayer in both models, were analysed using high-performance liquid chromatography (HPLC), as described previously (Li et al., 2013), to quantify the amount of compound in the sample. Prior to analysis, one volume of collected sample was mixed with ACN or MeOH for amoxicillin to precipitate the BSA. After centrifugation at 16000*g* for 10 min, the supernatant was injected in the HPLC column for analysis. Antipyrine and ketoprofen samples (50 μL) were applied to a C18 reverse-phase column (150 mm × 4.6 I.D, 5 μm particle size) with a guard column (7.5 mm × 4.6 mm I.D.; Alltech, The Netherlands) and detected by a UV detector (Perkin-Elmer, Waltham, MA) at 260 (antipyrine) and 254 (ketoprofen) nm. Digoxin (100 μL) and amoxicillin (50 μL) samples were injected to the same column and was detected and quantified by UV absorption (Waters, Milford, MA) at 220 and 245 nm, respectively. Trifluoroacetic acid (TFA) 1% in water (solvent A) and ACN (solvent B) were used as the mobile phase for analysis of all test compounds. For analysis of antipyrine, ketoprofen and amoxicillin, elution was applied at a flow rate of 1.0 mL/min, starting at 90% solvent A with a linear decrease to 0% solvent A in 20 min. Then, the gradient returned to the initial concentration in 2 min, which was maintained for 10 min before the next sample was injected. For the analysis of digoxin, the gradient elution started with 78% solvent A at a flow rate of 0.7 mL/min for 2 min, followed by a linear decrease to 0% solvent A in 8 min. Then, the gradient returned to the initial conditions by a linear gradient over 2 min and remained at this condition for 10 min. Calibration curves were made using commercially available reference compounds for each individual set of samples to enable quantification of the obtained results.

In the case of the amoxicillin studies with cells, liquid chromatography–mass spectrometry (LC-MS), was used to detect the amount of amoxicillin in the samples. Briefly, a 250 μL aliquot of the basolateral Transwell samples or 25 μL of gut-on-chip samples and apical Transwell samples was mixed with 10 μL of internal standard working solution (25 μg/L AMOX-d4). Then, 2 mL of ACN was added and the solution was placed in a rotary tumbler for 15 min followed by centrifugation at 3500*g* for 10 min. After that, ACN was evaporated with N_2 at 40 °C and the remaining pellet was re-suspended with either 100 μL 25 (*v*/v)% MeOH for the basolateral Transwell samples or 200 μL for the basolateral gut-on-chip samples. For the apical samples, evaporation was not necessary because of their higher concentrations. For all samples 100 μL was diluted with 900 μL 25% MeOH, and transferred to LC-MS/MS vials. Five μL of the sample was injected into the Acquity liquid chromatographic separation system (Waters, Milford, MA,) through an Acquity UPLC HSS T3 column (2.1 mm × 100 mm I.D., 1.8 μm) (Waters) at 30 °C employed under the gradient mixture of 0.001 (v/v)% formic acid in water (A) and 0.001 (v/v)% formic acid in ACN (B) at a flow rate of 0.4 mL/min. The gradient program was as follows: 0–1 min 0% B; 1–2.5 min, from 0 to 25% B; 2.5–5.4 min, from 25 to 70% B; 5.4–5.5 min, from 70 to 100% B; 5.5–8.5 min, 100% B; 8.5–8.6 min, from 100 to 0% B; followed by the re-equilibration at 0% B for 0.9 min before the next injection. The LC eluent was introduced directly into the electrospray ionization source (ESI) of the Q-Trap6500 mass spectrometer (Sciex, Framingham, MA) operating in the negative mode. Nitrogen was used as nebulizing turbo spray gas. The operational parameters of the ESI turbo ion source were as follows: vaporizing temperature 450 °C; curtain gas 35; and ionspray voltage −4000 V. Compound fragmentation was achieved using collision induced dissociation using N_2 as collision gas. The following multiple reaction

monitoring (MRM) transitions were used; the precursor ion [M- + H]- + for amoxicillin was measured at *m/z* 363.9 and the corresponding product ions were measured at m/z 222.9 and m/z 206. The declustering potential (DP) was set at −15 V and the collision energy (CE) was −14 V and −24 V, respectively. The precursor ion [M- + H]- + for amoxicillin-d4 was measured at m/z 367.9 and the product ion was m/z 227.0. The DP was −45 V, and CE was −14 V. Data processing was carried out using Multiquant software V3.0.2 (Sciex, Framingham, MA). For quantification, the peak areas of the target ions were corrected with those of the internal standard and the concentrations were determined using a matrix matched calibration line.

2.11. Statistical analysis

All statistical evaluations were evaluated using an independent paired *t*-test (SPSS, IBM). A *p*-value of ≤ 0.05 was considered significant.

3. Results

3.1. Simulated shear stress in the microfluidic gut-on-chip device

For the gut-on-chip experiments, the chip was placed in a chip holder connected to an eight-channel pump system (for four chips) with a flow sensor for every channel, allowing precise control of the apical (AP) and basolateral (BL) flow (Fig. 1A). Computational fluid dynamics were used to calculate and visualize the shear stress and flow velocity changes over the geometry of the microfluidic device. As can be seen in Fig. 1B, the flow velocity is highest near the inlet and decreases as the microchannels broaden until their maximal width (11 mm). In addition, due to an increment in the height of the chamber, the flow velocity was the lowest at the centre of the chamber. The shear stress at the cell culture surface area was calculated at ~0.0002–0.0017 dyn/cm^2.

3.2. Caco-2 cell monolayer integrity

Caco-2 cells were grown on the membrane in both the gut-on-chip and the Transwell model. Lucifer yellow was used as a fluorescent marker to monitor the integrity of the tight junctions between the Caco-2 cells. As shown in Fig. 2 the paracellular permeability value (P_{app}) of lucifer yellow decreased in time in both tested systems. Both systems demonstrated a tight monolayer after ~9 days of culture, but the P_{app} in the gut-on-chip appeared to fluctuate more in the first week of culture. After 9 days of culture, the permeability of lucifer yellow was stable and not significantly different between both systems (1.10×10^{-6}, 0.76×10^{-6}, 0.40×10^{-6} for the Transwell at day 9, 11, 15 and 0.72×10^{-6}, 0.54×10^{-6}, 0.64×10^{-6} cm/s for the gut-on-chip at day 9, 11, 14;$P > .05$; Independent *t*-test).

3.3. Assessment of cellular morphology

Caco-2 cells were cultured under continuous flow or static conditions for 21 days, in a gut-on-chip or Transwell, respectively. The cellular morphology was analysed using confocal microscopy, and representative images are shown in Fig. 3. Caco-2 cells grown under both conditions formed a comparable pattern of tight junctions, indicating monolayer formation, at day 5 to day 21 (Fig. 3A and B). By creating *Z*-stacks vertical cross-sections of the monolayers were assessed (Fig. 3C and D). Visual inspection showed an increase in the height of the monolayers in time in both systems, reaching ~10 μm at day 21. Marked differences between both culture systems became apparent in the subcellular localization of actin filaments after ~11 days of culturing. Monolayers grown under static conditions mainly expressed actin at the apical side, but cells grown under dynamic conditions exhibited more pronounced actin filaments located along the entire height of the cells including the basolateral side of the cells, were the cells were attached to the supporting porous membrane (Fig. 3E and F).

3.4. Caco-2 cell differentiation

The functional development of the cells in both the gut-on-chip and Transwell model was assessed by determining the ALP activity of the cells. ALP activity is an established marker of epithelial cell differentiation (Zucco et al., 2005; Jumarie and Malo, 1994; Ferruzza et al., 2012). The ALP activity of the cells grown under both conditions are shown in Fig. 4. Cells grown in the gut-on-chip system showed an increase in ALP activity in time, albeit with some fluctuations. At day 21, the ALP activity reached 15.2 ± 5.5 nmol/mg protein/min. Cells grown under static conditions also exhibited an increase in ALP activity in time, reaching 11.4 ± 4.5 nmol/mg protein/min. There were no significant differences in cellular ALP activity between the Caco-2 cells grown in the Transwell and gut-on-chip system at each individual time point ($P > .05$; Independent *t*-test).

3.5. Selection of non-cytotoxic concentrations of drugs

The MTT assay was used to select non-toxic concentrations of compounds to be applied in the subsequent transport studies. Proliferating (1 day old) cells were exposed to concentrations up to 500 μM, 300 μM, 250 μM and 500 μM of antipyrine, ketoprofen, digoxin, and amoxicillin, respectively, for 24 h. As shown in Fig. 5, no cytotoxicity (> 80% viability) was observed for all compounds at the highest tested concentrations.

3.6. Comparative drug transport under static and dynamic flow conditions

Compound translocation studies across Caco-2 cell monolayers

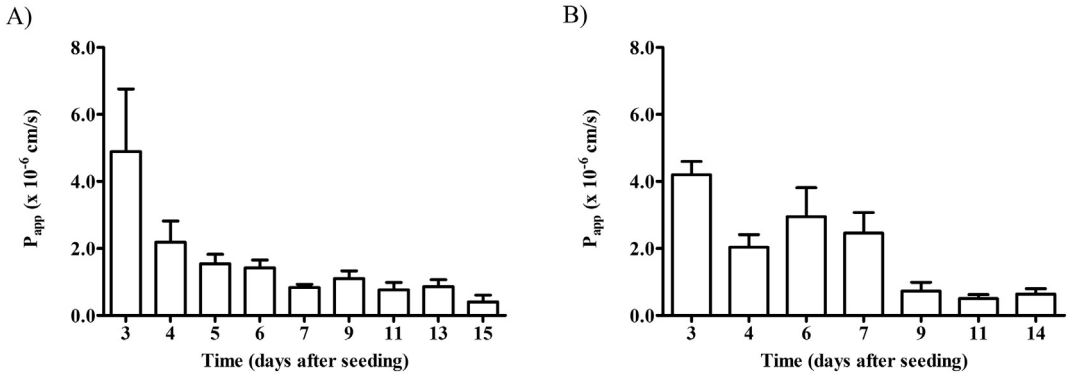

Fig. 2. Time dependent P_{app} (apparent permeability constant) reflecting tight junction integrity of a Caco-2 cell monolayer determined by measuring the paracellular translocation of lucifer yellow in a Transwell system A), and a gut-on-chip system B). The values are presented as means ± SEM; $n = 3$ and 7 (Transwell and gut-on-chip).

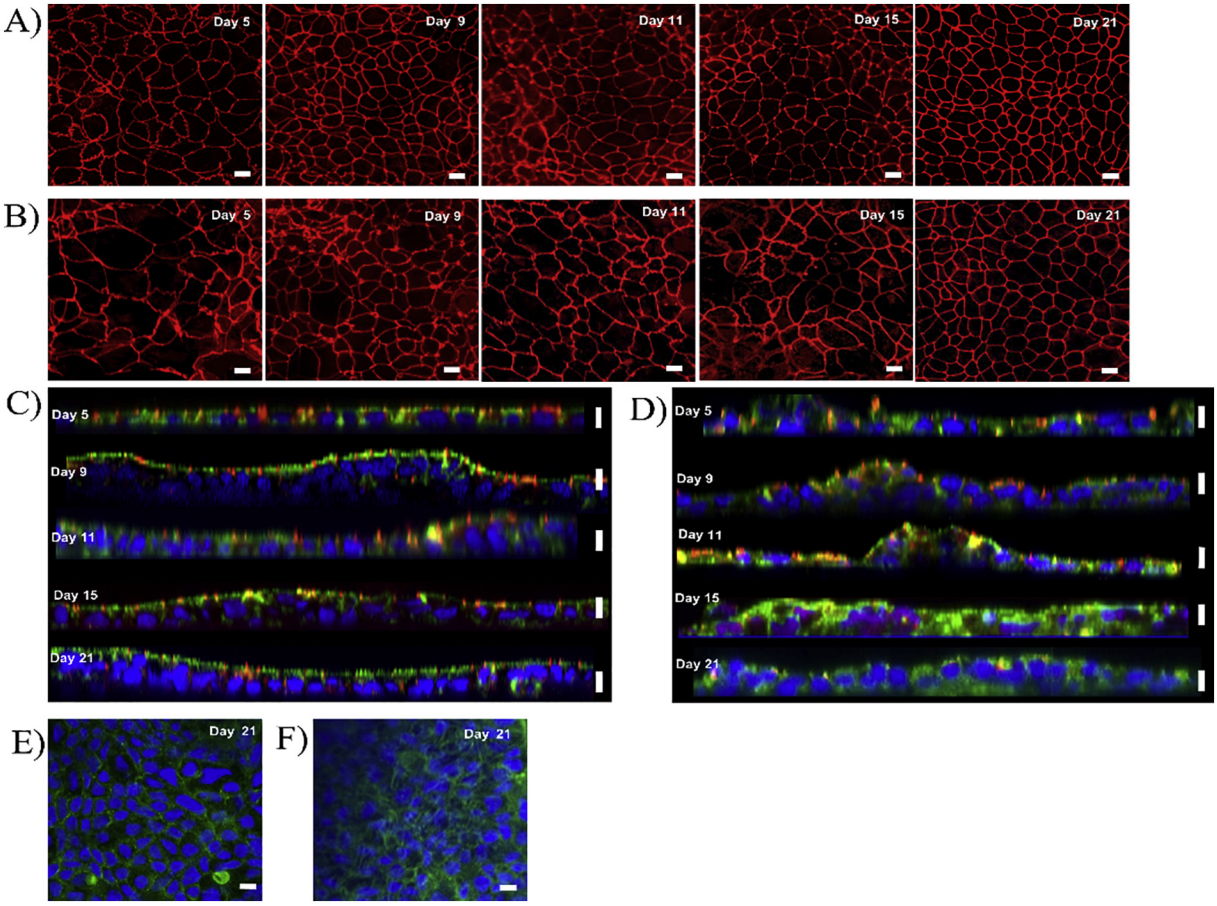

Fig. 3. Morphology of Caco-2 cells cultured for 21 days in a static Transwell system or in a gut-on-chip system under a continuous flow of 100 μL/h, visualized by confocal microscopy. Top views of the cell layer showing comparable tight junction patterns (ZO-1/TJP1) in red over a culture period of 21 days in A) a Transwell and in B) a gut-on-chip. Vertical cross-sections of the cell monolayer showing actin filaments (Phalloidin) in green, cell nuclei (DAPI) in blue, and tight junctions (ZO-1/TJP1) in red in C) a Transwell and D) a gut-on-chip. Note the increase in actin filaments over the entire cell height in the gut-on-chip *versus* the Transwell. Horizontal cross-sections at the basolateral side of the cells in E) a Transwell and F) a gut-on-chip further demonstrate the pronounced basolateral presence of actin (Phalloidin; green) in the Transwell *versus* gut-on-chip. The scale bar represents 10 μm. (For interpretation of the references to colour in this figure legend, the reader is referred to the web version of this article.)

grown under dynamic (gut-on-chip) and static (Transwell) conditions were performed 21 days after seeding of the cells. The transport of the compounds, antipyrine, ketoprofen, digoxin and amoxicillin, was determined using HPLC or LC-MS. A recovery of 83–118% for all measurements indicated little loss of compounds due to non-specific binding to the hardware or chemical instability.

The transport of the highly translocated compounds; antipyrine, ketoprofen, and digoxin was significantly lower in the gut-on-chip (P_{app} = 5.4 × 10^{-6}, 5.9 × 10^{-6} and 8.8 × 10^{-6} cm/s; $p < .05$) than in the Transwell (P_{app} = 22.7 × 10^{-6}, 16.0 × 10^{-6} and 16.4 × 10^{-6} cm/s) (Fig. 6A-C, and Table 1). Whereas the transport of the lowly translocated compound, amoxicillin appeared slightly higher in the gut-on-chip (P_{app} = 5.8 × 10^{-7} cm/s) *versus* the Transwell (P_{app} = 1.1 × 10^{-7} cm/s), although this difference was not significant ($p > .05$) (Fig. 6D and Table 1). To examine the influence of solely the system (*i.e.* Transwell *vs.* gut-on-chip) on the transport behaviour of the

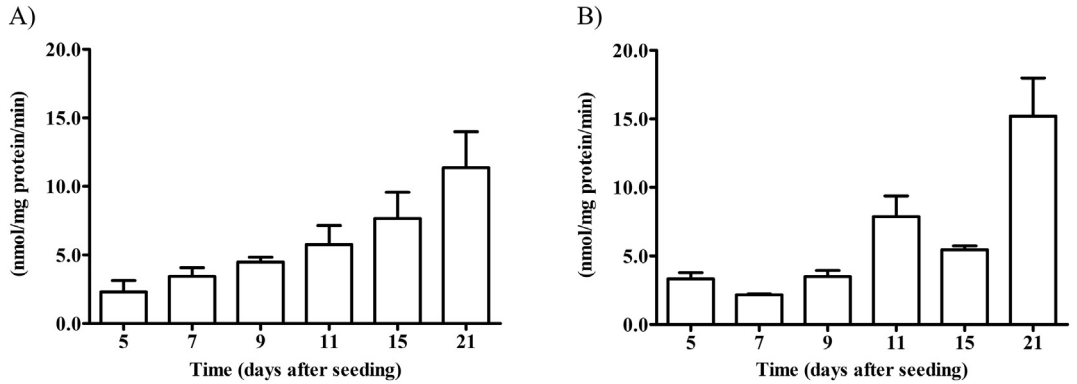

Fig. 4. ALP activity in Caco-2 cells grown in Transwell A) or gut-on-chip B). The values are presented as means ± SEM; n = 3 and 4 for Transwell and gut-on-chip, respectively.

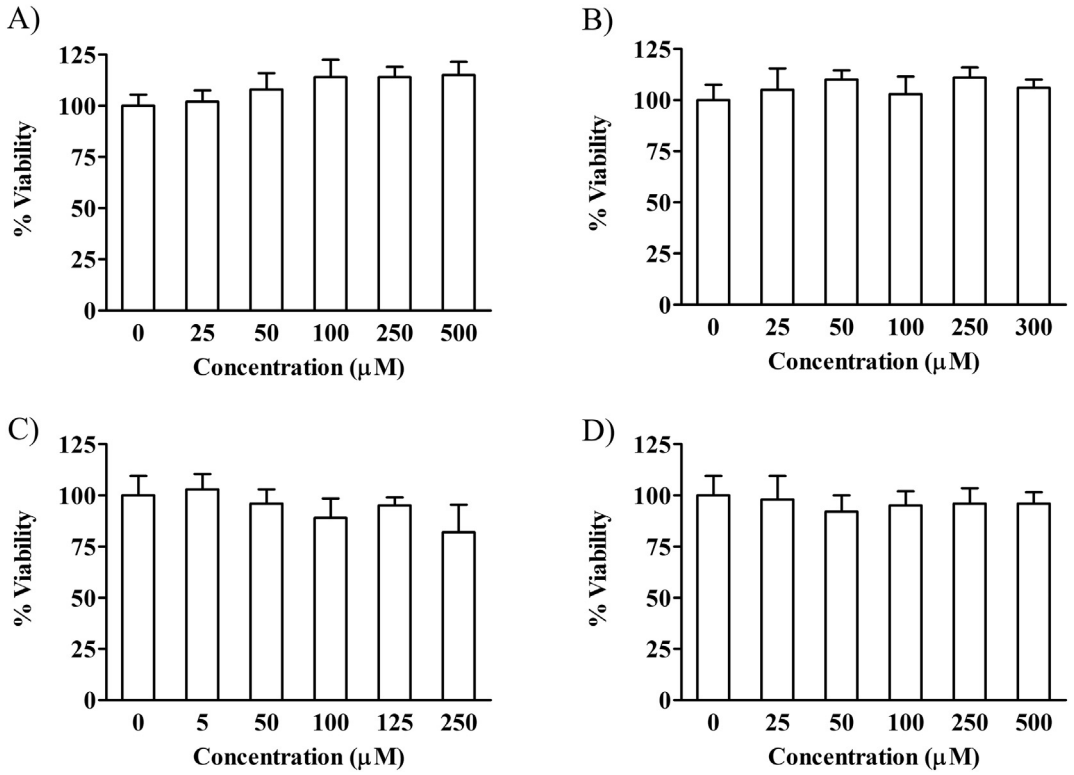

Fig. 5. Cell viability of 1-day old Caco-2 cells exposed for 24 h to increasing concentrations of A) antipyrine, B) ketoprofen, C) digoxin, and D) amoxicillin, given as a percentage (± SEM) of the negative control (n = 4).

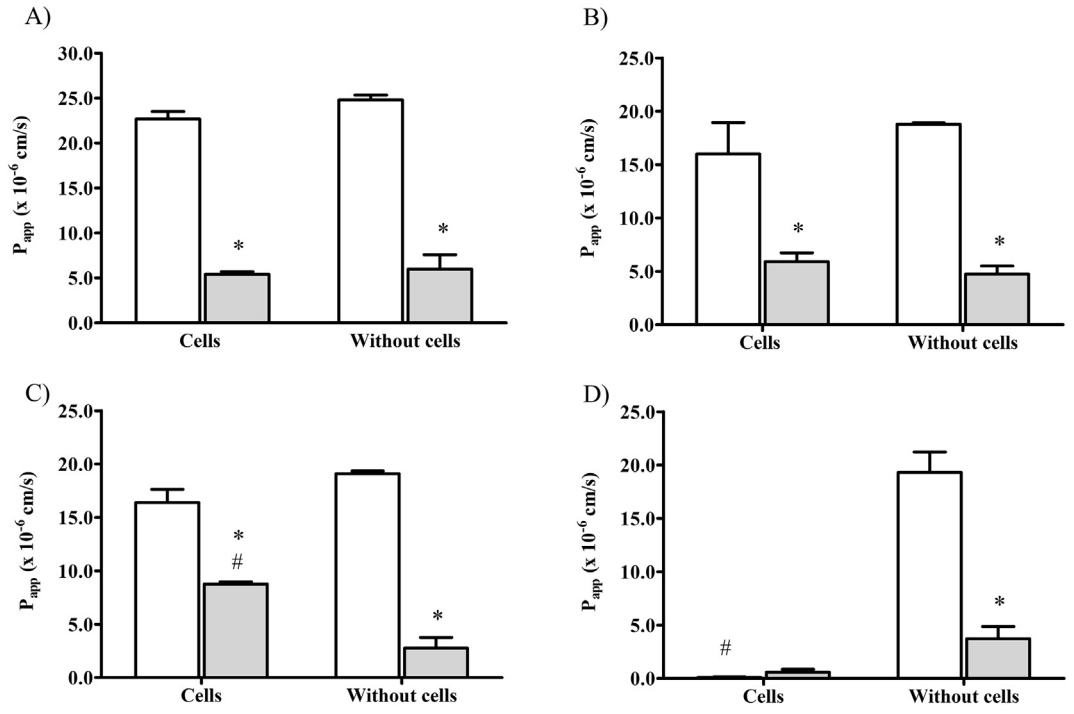

Fig. 6. Apparent permeability (P_{app}) values (± SEM) of model compounds; A) antipyrine, B) ketoprofen, C) digoxin, and D) amoxicillin under static Transwell (open bare), or dynamic gut-on-chip (gray bar) conditions, with or without 21-day old Caco-2 cells cultured on the porous membrane.* significant difference compared with the static Transwell (p < .05); # significant difference compared with the without cells condition (p < .05); (n = 3; antipyrine, digoxin, and amoxicillin); (n = 5; ketoprofen in gut-on-chip system).

compounds, both Transwell and gut-on-chip were also exposed to the compounds without cells.

Diffusion (expressed as P_{app}) of all four compounds across the membranes in both the gut-on-chip under dynamic conditions and Transwell (static conditions) without Caco-2 cell monolayers was significantly lower under dynamic flow in the gut-on-chip compared to the Transwell (*i.e.* four to seven-fold lower) (Fig. 6). Antipyrine and ketoprofen tested without cells showed translocation values that were

Table 1
Overview of the apparent permeability values (P_{app}) (± SEM) of the selected compounds in Caco2-cells cultured under static (Transwell) and dynamic (gut-on-chip) conditions in this study, and *in vitro* and *in vivo* Papp values or ranges (obtained from literature).

Compound	P_{app} ($\times 10^{-6}$ cm/s)		Literature *in vitro* Transwell P_{app} ($\times 10^{-6}$cm/s)	Human *in vivo* P_{app} ($\times 10^{-6}$cm/s)	BSC class	Fa (%)
	Transwell	Gut-on-chip				
Antipyrine	22.7 ± 0.5	5.4 ± 0.2	11.3–150.0[a]	560[d]	I[d]	100[d]
Ketoprofen	16.0 ± 1.6	5.9 ± 0.4	10.5–93.0[a]	870[d]	I[d]	100[d]
Digoxin	16.4 ± 0.7	8.8 ± 0.1	0.59–4.69[b]	N/A	II[e]	75[f]
Amoxicillin	0.11 ± 0.02	0.58 ± 0.2	0.021–1.8[c]	30[d]	III[d]	45-75[d]

BCS: Biopharmaceutics Classification System. Class I and II: high permeability, class III: low permeability.
Fa: human absorption of compounds.
[a] Data obtained from (Lee et al., 2017b).
[b] Data obtained from (Djnv and Nilsen, 2008; Elsby et al., 2008).
[c] Data obtained from (Jung et al., 2006; Irvine et al., 1999; Gres et al., 1998).
[d] Data obtained from (Lennernas, 2014).
[e] Data obtained from (Wu and Benet, 2005).
[f] Data obtained from (Takenaka et al., 2016). N/A: not available *in vivo* literature.

comparable to those obtained in the experiments with cells; antipyrine (Transwell; $P_{app} = 24.8 \times 10^{-6}$ cm/s, gut-on-chip; $P_{app} = 6.0 \times 10^{-6}$) and ketoprofen (Transwell; $P_{app} = 18.8 \times 10^{-6}$ cm/s, gut-on-chip; $P_{app} = 4.7 \times 10^{-6}$ cm/s). The transport of digoxin through the membrane without cells was also comparable with the transport through the membrane with cells in the Transwell ($P_{app} = 19.1 \times 10^{-6}$ cm/s). In the gut-on-chip the transport of digoxin was significantly lower without cells ($P_{app} = 2.8 \times 10^{-6}$ cm/s). Amoxicillin showed an increased translocation through the membrane without cells in both the Transwell and gut-on-chip (Transwell; $P_{app} = 19.3 \times 10^{-6}$ cm/s, gut-on-chip; $P_{app} = 3.7 \times 10^{-6}$ cm/s).

As the diffusion of the four compounds in the gut-on-chip system under dynamic conditions was lower than in the Transwell system as demonstrated by our experiments without the Caco-2 monolayers, the influence of the liquid flow in the gut-on-chip on the transport of antipyrine was examined. For this we examined the transport of antipyrine in gut-on-chip with cells, with or without flow. Without the flow, antipyrine showed a two-fold increased transport ($P_{app} = 10.4 \times 10^{-6}$ cm/s) compared to the transport with the flow ($P_{app} = 5.4 \times 10^{-6}$ cm/s), but the transport was still two-fold lower than in the Transwell system ($P_{app} = 22.7 \times 10^{-6}$ cm/s) (Fig. 7). The transport of all four compounds was also tested in the gut-on-chip and Transwell system without cells and without flow, showing approximately 2-fold lower P_{app} values for all compounds in the gut-on-chip system (Suppl. Table 1).

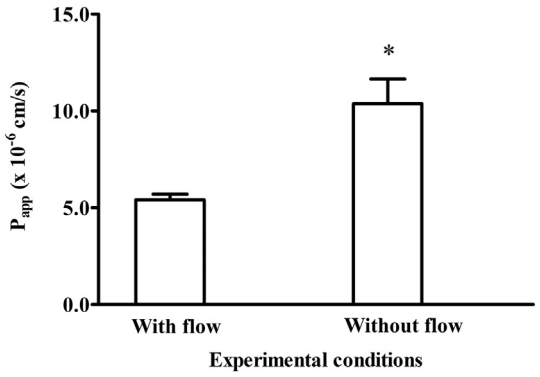

Fig. 7. Apparent permeability (P_{app}) values (± SEM) of antipyrine in the gut-on-chip system with 21-day old Caco-2 cells, under dynamic (with flow), or under static (without flow) conditions.* significant difference compared with dynamic conditions ($p < .05$); ($n = 3$).

4. Discussion

We aimed to evaluate whether our *in vitro* gut-on-chip intestinal barrier model is an adequate model for compound translocation studies. For this, we performed a biokinetic study comparing our dynamic gut-on-chip (Kulthong et al., 2018) with a conventional model using the static Transwell model. In both systems comparable trends in compound specific P_{app} values were observed. However, we observed marked differences in absolute transport rates in the Transwell *versus* the gut-on-chip model that most likely were caused by differences in experimental conditions and the design and intrinsic characteristics of the microfluidic chip.

In this study we used glass two-chamber microfluidic chips separated by a PET membrane on which we cultured epithelial cells (Caco-2) under dynamic conditions. Using a largely glass based microfluidic chip avoids the often raised issue of compound binding to PDMS based chips (van Meer et al., 2017). We successfully observed a high recovery of compounds as we have also shown previously for highly lipophilic compounds (Kulthong et al., 2018) indicating that no compounds were lost in the total chip setup, that includes tubing with a relatively large surface area.

To perform biokinetic studies, conventionally Caco-2 cells are used after 21 days of culturing in Transwell systems, when they have developed into a tight monolayer of differentiated cells (Artursson et al., 2001). We assessed the cell layer integrity in the conventional Transwell model *versus* the gut-on-chip model by exposing monolayers of cells to a marker for paracellular transport (lucifer yellow). The paracellular translocation dropped quickly for the Caco-2 monolayers in the Transwell model reaching stable low levels in the second week of culturing. A similar trend, albeit more variable, was observed for the Caco-2 monolayers grown under dynamic flow conditions in the chip. Previously, other research groups have characterized Caco-2 cell layer integrity and differentiation in microfluidic chips, but in chips with different designs. Using microfluidic chips with a narrow long channel, full maturation of the cell monolayer and barrier integrity was observed already after 3–5 days of seeding (Kim et al., 2012; Chi et al., 2015), which is faster than observed in our model. Next we evaluated the differentiation of the Caco-2 cells in both the gut-on-chip and Transwell by determining ALP activity, a known marker for intestinal cell differentiation (Jumarie and Malo, 1994; Ferruzza et al., 2012; Zucco et al., 2005). Caco-2 cell differentiation was comparable in both systems, ALP activity increased upon increasing the culture period with a maximum activity reached on day 21. Again, in a chip with a narrow elongated channel, it was observed that brush border aminopeptidase activity already on day 3-5 reached the same level as following 21 days of culturing in Transwell (Kim et al., 2012, Chi et al., 2015). Due to the differences in chip design the resulting shear stress experienced by the

cells is different in this chip system as compared to ours. In our device, we estimated a shear stress of approximately 0.0002–0.0017 dyn/cm^2 which is lower compared to the 0.02 dyn/cm^2 reported for the channel chips (Kim et al., 2012). Literature data on *in vivo* shear stress in the gut however report highly variable ranges, between ~0.002–12.0 dyn/cm^2 (Kim et al., 2012; Guo et al., 2000; Hardacre et al., 2016), depending on the intestinal location and viscosity of digesta. Therefore, to mimic the real shear stress experience by epithelial cells within the intestinal lumen is still challenging *in vitro*. Lastly, we have evaluated the monolayer morphology of Caco-2 cells grown in the gut-on-chip and static Transwell using confocal microscopy. While the cell height was comparable, cells grown under constant flow expressed more actin filaments on the basolateral side compared to cells grown under static conditions, as shown before (Kulthong et al., 2018). Actin filaments are associated with cell adhesion and mechanics, remodelling of actin filaments might alter cell spread, migration, elongation, or enlargement of the cells (Noria et al., 2004; Miura et al., 2015). The remodelling of the actin filaments did not affect the barrier integrity in the gut-on-chip model.

We exposed differentiated monolayers of Caco-2 cells, grown under dynamic flow conditions in the gut-on-chip and under static conditions in the Transwell system, to four model compounds representing high and low permeability compound classes (Biopharmaceuticals Classification System (BCS). Monolayers of differentiated Caco-2 cells are regarded representative for the gastrointestinal absorption of compounds *in vivo* with the best correlation for drugs transported by the passive transcellular route (Cheng et al., 2008; Artursson et al., 2001). The highly transported compounds antipyrine, ketoprofen and digoxin indeed showed high P_{app} values in both systems. Amoxicillin, a low transported compound, showed low P_{app} values in both systems. The P_{app} values derived from the static experiment were in line with those previously obtained from static *in vitro* Caco-2 experiments for antipyrine, ketoprofen and amoxicillin (see Table 1 and references therein). Our digoxin P_{app} value was higher, in both the Transwell and gut-on-chip system than those reported before. This difference likely can be explained by the variable expression of P-glycoprotein 1 by Caco-2 cells, this efflux transporter is responsible for the cellular excretion of digoxin. Variable expression levels can depend on the passage number of the cultured cells (Goto et al., 2003). The P_{app} values of the high permeability (class I) compounds antipyrine and ketoprofen were about 4.2 and 2.7 folds lower, respectively, when evaluated using Caco-2 cells under dynamic flow conditions in the gut-on-chip compared to Caco-2 cells under static conditions in Transwell. Given the outcome of our experiments without cells and without flow, we conclude that these differences can be explained by (laminar) flow related effects and by influence of the design of the chip and/or the material of the membrane on diffusion of these compounds. Laminar flow is the fluid flow that occurs in long thin parallel layers with no disruption between them and can be defined by the Reynolds number. The Reynolds number is the ratio of internal force to viscous force. For our gut-on-chip conditions the Reynolds number equals ~0.007. At low Reynolds numbers, viscous forces dominate, which implies a low migration (or diffusion) of dissolved chemicals across layers resulting in less contact of the compounds with the cell surface (Sosa-Hernandez et al., 2018; Christoffersson, 2018). In the absence of flow, diffusion is facilitated, this is demonstrated by the ~2 times higher P_{app} value of antipyrine in the gut-on-chip with cells without flow *versus* with flow. Nevertheless, the P_{app} value in the gut-on-chip with cells and without flow was still lower than that in the Transwell. The use of different membranes and the influence of different designs (*i.e.* apical and basolateral volumes) in the gut-on-chip and Transwell models could have contributed to these observed differences as shown by static experiments using both membranes.

Monolayers of Caco-2 cells, are a standard model used to categorize drugs into the four classes of the Biopharmaceuticals Classification System (BCS) and to predict intestinal absorption of compounds (Smetanova et al., 2011; Miret et al., 2004). However, in the literature reported (apparent) permeability values of compounds *in vitro* vary between labs and are lower than those reported for human *in vivo* (Table 1). The latter usually is explained by the higher TEER values *in vitro* compared to TEER values *in vivo* (Lennernas, 1998; Lee et al., 2017b; Artursson et al., 2001). Therefore, relative correlation values between *in vitro* and human data have been often used to evaluate the prediction potential of new *in vitro* models and to predict whether absorption of compounds in human will be high or low (Irvine et al., 1999; Li et al., 2007; Marino et al., 2005; Takenaka et al., 2016). The transport data in our study are consistent with the BCS compound classification, showing higher transport of antipyrine, ketoprofen, and digoxin than amoxicillin.

Compound translocation of the four model compounds in the gut-on-chip and Transwell are in line with the compound Biopharmaceuticals Classification System, albeit absolute P_{app} values of class I and II compounds were markedly lower in the gut-on-chip. Clearly the laminar fluid flow in the microfluidic chip affects the transport of compounds, by limiting the diffusions of compounds towards the membrane. A solution can be to incorporate herringbone-shaped groves to allow mixing as shown by (de Haan et al., 2019). Secondly, the shape of the cell compartment affects the shear force and liquid flow patterns. The consequences of these design characteristics, and thus accompanying shear forces, on cell morphology, cell physiology, and cell differentiation and on how this affects compound transport still needs to be assessed. Comparative studies on monolayer morphology related to chip design are emerging (Bein et al., 2018).

In conclusion, different P_{app} values of the tested compounds were obtained in the gut-on-chip and Transwell models for antipyrine, ketoprofen, and digoxin. The P_{app} value obtained for the low permeability compound amoxicillin was comparable in both models. These results are in line with the compound Biopharmaceuticals Classification System. Thus, both the gut-on-chip and the Transwell model can be used for transport studies of chemicals. The gut-on-chip model allows for integration with on line detection of compounds (Santbergen et al., 2020) while the classical static Transwell model is easier to use.

Declaration of Competing Interest

The authors state no conflict of interest.

Acknowledgement

The authors sincerely acknowledge the support and assistance of prof.dr.ir. IMCM (Ivonne) Rietjens. K. K. is supported by a Royal Thai government Scholarship. This work was in part supported by the Dutch Ministry of Agriculture, Nature and Food Quality (project KB-23-002-022).

Appendix A. Supplementary data

Supplementary data to this article can be found online at https://doi.org/10.1016/j.tiv.2020.104815.

References

Artursson, P., Palm, K., Luthman, K., 2001. Caco-2 monolayers in experimental and theoretical predictions of drug transport (reprinted from advanced drug delivery reviews, vol 22, pg 67-84, 1996). Adv. Drug Deliv. Rev. 46, 27–43 (2001).

Barata, D., VAN Blitterswijk, C., Habibovic, P., 2016. High-throughput screening approaches and combinatorial development of biomaterials using microfluidics. Acta Biomater. 34, 1–20.

Bein, A., Shin, W., Jalili-Firoozinezhad, S., Park, M.H., Sontheimer-Phelps, A., Tovaglieri, A., Chalkiadaki, A., Kim, H.J., Ingber, D.E., 2018. Microfluidic organ-on-a-chip models of human intestine. Cell. Mol. Gastroenterol. Hepatol. 5, 659–668.

Berthier, E., Young, E.W.K., Beebe, D., 2012. Engineers are from PDMS-land, biologists are from polystyrenia. Lab Chip 12, 1224–1237.

Cao, L., Kuratnik, A., Xu, W.L., Gibson, J.D., Kolling, F., Falcone, E.R., Ammar, M., Van

Heyst, M.D., Wright, D.L., Nelson, C.E., Giardina, C., 2015. Development of intestinal organoids as tissue surrogates: cell composition and the epigenetic control of differentiation. Mol. Carcinog. 54, 189–202.
Cheng, K.C., Li, C., Uss, A.S., 2008. Prediction of oral drug absorption in humans - from cultured cell lines and experimental animals. Expert Opin. Drug Metab. Toxicol. 4, 581–590.
Chi, M., Yi, B., Oh, S., Park, D.J., Sung, J.H., Park, S., 2015. A microfluidic cell culture device (muFCCD) to culture epithelial cells with physiological and morphological properties that mimic those of the human intestine. Biomed. Microdevices 17, 9966.
Christoffersson, J., 2018. *Organs-on-Chips for the Pharmaceutical Development Process: Design Perspectives and Implementations* Doctoral Thesis. Linköping University.
DE Haan, P., Ianovska, M.A., Mathwig, K., VAN Lieshout, G.A.A., Triantis, V., Bouwmeester, H., Verpoorte, E., 2019. Digestion-on-a-chip: a continuous-flow modular microsystem recreating enzymatic digestion in the gastrointestinal tract. Lab Chip 19, 1599–1609.
Djnv, A., Nilsen, O.G., 2008. Caco-2 cell methodology and inhibition of the P-glycoprotein transport of digoxin by aloe vera juice. Phytother. Res. 22, 1623–1628.
Eisenbrand, G., Pool-Zobel, B., Baker, V., Balls, M., Blaauboer, B.J., Boobis, A., Carere, A., Kevekordes, S., Lhuguenot, J.C., Pieters, R., Kleiner, J., 2002. Methods of in vitro toxicology. Food Chem. Toxicol. 40, 193–236.
Elsby, R., Surry, D.D., Smith, V.N., Gray, A.J., 2008. Validation and application of Caco-2 assays for the in vitro evaluation of development candidate drugs as substrates or inhibitors of P-glycoprotein to support regulatory submissions. Xenobiotica 38, 1140–1164.
Ferruzza, S., Rossi, C., Scarino, M.L., Sambuy, Y., 2012. A protocol for differentiation of human intestinal Caco-2 cells in asymmetric serum-containing medium. Toxicol. in Vitro 26, 1252–1255.
Gao, D., Liu, H.X., Lin, J.M., Wang, Y.N., Jiang, Y.Y., 2013. Characterization of drug permeability in Caco-2 monolayers by mass spectrometry on a membrane-based microfluidic device. Lab Chip 13, 978–985.
Goto, M., Masuda, S., Saito, H., Inui, K., 2003. Decreased expression of P-glycoprotein during differentiation in the human intestinal cell line Caco-2. Biochem. Pharmacol. 66, 163–170.
Gres, M.C., Julian, B., Bourrie, M., Meunier, V., Roques, C., Berger, M., Boulenc, X., Berger, Y., Fabre, G., 1998. Correlation between oral drug absorption in humans, and apparent drug permeability in TC-7 cells, a human epithelial intestinal cell line: comparison with the parental Caco-2 cell line. Pharm. Res. 15, 726–733.
Guerra, A., Campillo, N.E., Paez, J.A., 2010. Neural computational prediction of oral drug absorption based on CODES 2D descriptors. Eur. J. Med. Chem. 45, 930–940.
Guo, P., Weinstein, A.M., Weinbaum, S., 2000. A hydrodynamic mechanosensory hypothesis for brush border microvilli. Am. J. Phys. Renal Phys. 279, F698–F712.
Gupta, N., Liu, J.R., Patel, B., Solomon, D.E., Vaidya, B., Gupta, V., 2016. Microfluidics-based 3D cell culture models: utility in novel drug discovery and delivery research. Bioeng. Transl. Med. 1, 63–81.
Hardacre, A.K., Lentle, R.G., Yap, S.Y., Monro, J.A., 2016. Does viscosity or structure govern the rate at which starch granules are digested? Carbohydr. Polym. 136, 667–675.
Hirama, H., Satoh, T., Sugiura, S., Shin, K., Onuki-Nagasaki, R., Kanamori, T., Inoue, T., 2019. Glass-based organ-on-a-chip device for restricting small molecular absorption. J. Biosci. Bioeng. 127 (5), 641–646. https://doi.org/10.1016/j.jbiosc.2018.10.019.
Hubatsch, I., Ragnarsson, E.G.E., Artursson, P., 2007. Determination of drug permeability and prediction of drug absorption in Caco-2 monolayers. Nat. Protoc. 2, 2111–2119.
Imura, Y., Asano, Y., Sato, K., Yoshimura, E., 2009. A microfluidic system to evaluate intestinal absorption. Anal. Sci. 25, 1403–1407.
Irvine, J.D., Takahashi, L., Lockhart, K., Cheong, J., Tolan, J.W., Selick, H.E., Grove, J.R., 1999. MDCK (Madin-Darby canine kidney) cells: A tool for membrane permeability screening. J. Pharm. Sci. 88, 28–33.
Jumarie, C., Malo, C., 1994. Alkaline-phosphatase and peptidase activities in Caco-2 cells - differential response to triiodothyronine. In Vitro Cell. Dev. Biol. Anim. 30A, 753–760.
Jung, S.J., Choi, S.O., Um, S.Y., Kim, J.I., Choo, H.Y.P., Choi, S.Y., Chung, S.Y., 2006. Prediction of the permeability of drugs through study on quantitative structure-permeability relationship. J. Pharm. Biomed. Anal. 41, 469–475.
Kauffman, A.L., Gyurdieva, A.V., Mabus, J.R., Ferguson, C., Yan, Z.Y., Hornby, P.J., 2013. Alternative functional in vitro models of human intestinal epithelia. Front. Pharmacol. 4.
Kim, H.J., Ingber, D.E., 2013. Gut-on-a-Chip microenvironment induces human intestinal cells to undergo villus differentiation. Integr. Biol. 5, 1130–1140.
Kim, H.J., Huh, D., Hamilton, G., Ingber, D.E., 2012. Human gut-on-a-chip inhabited by microbial flora that experiences intestinal peristalsis-like motions and flow. Lab Chip 12, 2165–2174.
Kimura, H., Yamamoto, T., Sakai, H., Sakai, Y., Fujii, T., 2008. An integrated microfluidic system for long-term perfusion culture and on-line monitoring of intestinal tissue models. Lab Chip 8, 741–746.
Kulthong, K., Duivenvoorde, L., Mizera, B.Z., Rijkers, D., ten Dam, G., Oegema, G., Puzyn, T., Bouwmeester, H., van der Zande, M., 2018. Implementation of a dynamic intestinal gut-on-a-chip barrier model for transport studies of lipophilic dioxin congeners. RSC Adv. 8, 32440–32453.
Lee, D.W., Ha, S.K., Choi, I., Sung, J.H., 2017a. 3D gut-liver chip with a PK model for prediction of first-pass metabolism. Biomed. Microdevices 19.
Lee, J.B., Zgair, A., Taha, D.A., Zang, X.W., Kagan, L., Kim, T.H., Kim, M.G., Yun, H.Y., Fischer, P.M., Gershkovich, P., 2017b. Quantitative analysis of lab-to-lab variability in Caco-2 permeability assays. Eur. J. Pharm. Biopharm. 114, 38–42.
Lennernas, H., 1998. Human intestinal permeability. J. Pharm. Sci. 87, 403–410.
Lennernas, H., 2014. Human in vivo regional intestinal permeability: importance for pharmaceutical drug development. Mol. Pharm. 11, 12–23.
Leppert, E.R., Smith, N.F., Cox, M.C., Scripture, C.D., Figg, W.D., 2006. Thalidomide metabolism and hydrolysis: mechanisms and implications. Curr. Drug Metab. 7, 677–685.
Li, C., Liu, T., Cui, X., Uss, A.S., Cheng, K.C., 2007. Development of in vitro pharmacokinetic screens using Caco-2, human hepatocyte, and Caco-2/human hepatocyte hybrid systems for the prediction of oral bioavailability in humans. J. Biomol. Screen. 12, 1084–1091.
Li, N.Z., Schwartz, M., Ionescu-Zanetti, C., 2009. PDMS compound adsorption in context. J. Biomol. Screen. 14, 194–202.
Li, H.Q., van Ravenzwaay, B., Rietjens, I.M.C.M., Louisse, J., 2013. Assessment of an in vitro transport model using BeWo b30 cells to predict placental transfer of compounds. Arch. Toxicol. 87, 1661–1669.
Mahler, G.J., Esch, M.B., Glahn, R.P., Shuler, M.L., 2009. Characterization of a gastrointestinal tract microscale cell culture analog used to predict drug toxicity. Biotechnol. Bioeng. 104, 193–205.
Marin, T.M., de Carvalho Indolfo, N., Rocco, S.A., Basei, F.L., de Carvalho, M., de Almeida Goncalves, K., Pagani, E., 2019. Acetaminophen absorption and metabolism in an intestine/liver microphysiological system. Chem. Biol. Interact. 299, 59–76.
Marino, A.M., Yarde, M., Patel, H., Chong, S.H., Balimane, P.V., 2005. Validation of the 96 well Caco-2 cell culture model for high throughput permeability assessment of discovery compounds. Int. J. Pharm. 297, 235–241.
Martignoni, M., Groothuis, G.M.M., DE Kanter, R., 2006. Species differences between mouse, rat, dog, monkey and human CYP-mediated drug metabolism, inhibition and induction. Expert Opin. Drug Metab. Toxicol. 2, 875–894.
Matthiessen, L., Lucaroni, B., Sachez, E., 2003. Towards responsible animal research Addressing the ethical dimension of animal experimentation and implementing the ?Three Rs? principle in biomedical research. EMBO Rep. 4 (2). https://doi.org/10.1038/sj.embor.embor745/abstract. *EMBO reports* [Online], 4. Available. (Accessed 01).
Mcdonald, J.C., Duffy, D.C., Anderson, J.R., Chiu, D.T., Wu, H., Schueller, O.J., Whitesides, G.M., 2000. Fabrication of microfluidic systems in poly(dimethylsiloxane). Electrophoresis 21, 27–40.
Miret, S., Abrahamse, L., DE Groene, E.M., 2004. Comparison of in vitro models for the prediction of compound absorption across the human intestinal mucosa. J. Biomol. Screen. 9, 598–606.
Miura, S., Sato, K., Kato-Negishi, M., Teshima, T., Takeuchi, S., 2015. Fluid shear triggers microvilli formation via mechanosensitive activation of TRPV6. Nat. Commun. 6, 8871.
Noria, S., Xu, F., Mccue, S., Jones, M., Gotlieb, A.I., Langille, B.L., 2004. Assembly and reorientation of stress fibers drives morphological changes to endothelial cells exposed to shear stress. Am. J. Pathol. 164, 1211–1223.
Ortmann, D., Vallier, L., 2017. Variability of human pluripotent stem cell lines. Curr. Opin. Genet. Dev. 46, 179–185.
Pocock, K., Delon, L., Bala, V., Rao, S., Priest, C., Prestidge, C., Thierry, B., 2017. Intestine-on-a-chip microfluidic model for efficient in vitro screening of oral chemotherapeutic uptake. ACS Biomater. Sci. Eng. 3, 951–959.
Rollin, B.E., 2003. Toxicology and new social ethics for animals. Toxicol. Pathol. 31 (Suppl), 128–131.
Russell, W.M.S., Burch, R.L., 1959. The Principles of Humane Experimental Technique, London, Methuen.
Santbergen, M.J.C., VAN DER Zande, M., Bouwmeester, H., Nielen, M.W.F., 2019. Online and in situ analysis of organs-on-a-chip. TrAC Trends Anal. Chem. 115, 138–146. https://doi.org/10.1016/j.trac.2019.04.006.
Santbergen, M.J.C., van der Zande, M., Gerssen, A., Bouwmeester, H., Nielen, M.W.F., 2020. Dynamic in vitro intestinal barrier model coupled to chip-based liquid chromatography mass spectrometry for oral bioavailability studies. Anal. Bioanal. Chem. 412, 1111–1122. https://doi.org/10.1007/s00216-019-02336-6.
Selimovic, S., Sim, W.Y., Kirn, S.B., Jang, Y.H., Lee, W.G., Khabiry, M., Bae, H., Jambovane, S., Hong, J.W., Khademhosseini, A., 2011. Generating nonlinear concentration gradients in microfluidic devices for cell studies. Anal. Chem. 83, 2020–2028.
Shim, K.Y., Lee, D., Han, J., Nguyen, N.T., Park, S., Sung, J.H., 2017. Microfluidic gut-on-a-chip with three-dimensional villi structure. Biomed. Microdevices 19.
Smetanova, L., Stetinova, V., Svoboda, Z., Kvetina, J., 2011. Caco-2 cells, biopharmaceutics classification system (BCS) and biowaiver. Acta Med. (Hradec Kralove) 54, 3–8.
Sosa-Hernandez, J.E., Villalba-Rodriguez, A.M., Romero-Castillo, K.D., Aguilar-Aguila-Isaias, M.A., Garcia-Reyes, I.E., Hernandez-Antonio, A., Ahmed, I., Sharma, A., Parra-Saldivar, R., Iqbal, H.M.N., 2018. Organs-on-a-chip module: A review from the development and applications perspective. Micromachines (Basel) 9.
Takenaka, T., Harada, N., Kuze, J., Chiba, M., Iwao, T., Matsunaga, T., 2016. Application of a human intestinal epithelial cell monolayer to the prediction of oral drug absorption in humans as a superior alternative to the Caco-2 cell monolayer. J. Pharm. Sci. 105, 915–924.
Tan, H.Y., Trier, S., Rahbek, U.L., Dufva, M., Kutter, J.P., Andresen, T.L., 2018. A multi-chamber microfluidic intestinal barrier model using Caco-2 cells for drug transport studies. PLoS One 13, e0197101.
Thangawng, A.L., Ruoff, R.S., Swartz, M.A., Glucksberg, M.R., 2007. An ultra-thin PDMS membrane as a bio/micro-nano interface: fabrication and characterization. Biomed. Microdevices 9, 587–595.
Tsao, C.W., 2016. Polymer microfluidics: simple, low-cost fabrication process bridging academic lab research to commercialized production. Micromachines 7.
van Meer, B.J., de Vries, H., Firth, K.S.A., van Weerd, J., Tertoolen, L.G.J., Karperien, H.B.J., Jonkheijm, P., Denning, C., Ijzerman, A.P., Mummery, C.L., 2017. Small molecule absorption by PDMS in the context of drug response bioassays. Biochem. Biophys. Res. Commun. 482, 323–328.

Workman, M.J., Gleeson, J.P., Troisi, E.J., Estrada, H.Q., Kerns, S.J., Hinojosa, C.D., Hamilton, G.A., Targan, S.R., Svendsen, C.N., Barrett, R.J., 2018. Enhanced utilization of induced pluripotent stem cell-derived human intestinal organoids using microengineered chips. Cell. Mol. Gastroenterol. Hepatol. 5 (669 − +.).

Wu, C.Y., Benet, L.Z., 2005. Predicting drug disposition via application of BCS: transport/absorption/elimination interplay and development of a biopharmaceutics drug disposition classification system. Pharm. Res. 22, 11–23.

Yeon, J.H., Park, J.K., 2009. Drug permeability assay using microhole-trapped cells in a microfluidic device. Anal. Chem. 81, 1944–1951.

Zhang, X., Huk, D.J., Wang, Q., Lincoln, J., Zhao, Y., 2014. A microfluidic shear device that accommodates parallel high and low stress zones within the same culturing chamber. Biomicrofluidics 8, 054106.

Zucco, F., Batto, A.F., Bises, G., Chambaz, J., Chiusolo, A., Consalvo, R., Cross, H., Dal Negro, G., De Angelis, I., Fabre, G., Guillou, F., Hoffman, S., Laplanche, L., Morel, E., Pincon-Raymond, M., Prieto, P., Turco, L., Ranaldi, G., Rousset, M., Sambuy, Y., Scarino, M.L., Torreilles, F., Stammati, A., 2005. An inter-laboratory study to evaluate the effects of medium composition on the differentiation and barrier function of Caco-2 cell lines. Altern. Lab. Anim 33, 603–618.